Linear magnetoresistance and weak antilocalization in a $LaVO_3/KTaO_3$ heterostructure

Harsha Silotia, Anamika Kumari, Amit Vashist,* and S. Chakraverty†
Quantum Materials and Devices Unit, Institute of Nano Science and Technology, Sector-81, Punjab, 140306, India

(Received 8 June 2023; revised 15 April 2024; accepted 21 May 2024; published 5 June 2024)

In this paper, we report a detailed magnetotransport study on the conducting interface formed by juxtaposed $LaVO_3$ (LVO) thin film on $KTaO_3$ (KTO) substrate. Magnetoresistance (MR) shows a crossover from quadratic dependence to linear dependence at critical applied magnetic fields (B^*) for both in-plane ($B \parallel I$) and out-of-plane ($B \perp I$) configurations. The negative magnetoresistance and parabolic dependence of the B^* on temperature suggests the presence of linear band dispersion. In addition to linear magnetoresistance (LMR) at high magnetic fields, we have also observed weak antilocalization (WAL) cusp in magnetoresistance at low magnetic fields and temperatures for both in-plane and out-of-plane field configurations. Maekawa-Fukuyama (MF) theory is used to analyze the WAL data, which indicates the presence of two conduction channels. Angle dependence of WAL analysis shows that the conducting channels are not restricted to two dimensions. Temperature-dependent study reveals the presence of electron-electron and electron-phonon scattering mechanisms. Our analysis suggests the presence of a quasi-two-dimensional electron gas with linear band dispersion at the interface of $LaVO_3$ and $KTaO_3$.

DOI: 10.1103/PhysRevB.109.245405

I. INTRODUCTION

The existence of Dirac/Weyl fermions in materials with degenerate linear band crossing near the Fermi level has generated a great amount of interest in the field of condensed matter physics. Peculiar transport properties exhibited by such materials fascinated the world not only because of their fundamental importance but also due to their technological applications in the field of spintronics [1–5]. They exhibit linear dispersion relation, evident by the large separation between the lowest and first Landau level. It has been shown that Dirac materials commonly exhibit well-known quantum physical properties in magnetotransport, which encompass quantum Hall effect (QHE), chiral anomaly induced negative magnetoresistance, nontrivial Berry phase, weak antilocalization (WAL), linear magnetoresistance, and many others [6–10]. The phenomenon of linear magnetoresistance (LMR) defies the conventional expectations of quadratic magnetoresistance (MR) typically observed in metals and semiconductors, presenting an intriguing and unusual behavior within condensed matter systems [11,12]. The origin of linear magnetoresistance (MR) can be attributed to either classical mechanisms or quantum phenomena [13–15]. In the classical model, disorder or mobility fluctuation plays a dominant role in LMR [16]. In contrast, linear magnetoresistance (MR) can also arise as a consequence of quantum effects occurring when all charge carriers become degenerate within the lowest Landau level (LL), specifically in the regime known as the quantum limit [17]. Such a kind of linear MR can be seen in topological materials and thus there is renewed interest to explore other materials such as single crystals, thin films, and heterostructures with similar observations [18–21]. Additionally, the quantum interference of the time-reversed scattering path in a high spin-orbit coupling compound may lead to the observation of WAL. WAL results in an enhancement (suppression) in conductivity (resistivity) at low magnetic fields and temperatures. The observation of WAL can be an important manifestation of the π Berry phase in topological materials.

Recently, topological band structure and Dirac cones have been observed in perovskite oxide materials [22–26]. Perovskite oxides, due to their novel physical properties and functionalities in appropriate heterostructures, are a very exciting class of materials [27–31]. Similar to the topological materials, perovskite oxides have attracted increasing attention due to their interesting properties including a planar Hall effect (PHE), and Shubnikov de Haas (SdH) oscillation at the interface of EuO/KTO with nontrivial π Berry phase [32] negative MR induced by chiral anomaly, linear positive magnetoresistance, and quantum oscillations in $SrRuO_3$ thin films grown on $SrTiO_3$ [25], topological Hall effects in $SrFeO_3$ [33], and so on. The availability of growth techniques accurate to the atomic level such as molecular beam epitaxy (MBE) and pulsed laser deposition (PLD) allowed us to explore quantum phenomena arising due to the interplay of orbital, charge, and spin degree of freedom. Recently, signatures of Adler-Bell-Jackiw (ABJ) anomaly or chiral anomaly and Weyl fermions have been observed at the interface of $LaVO_3/KTaO_3$ (LVO/KTO) [34], increasing interest in further study of this system. In this article, we have investigated temperature and angle-dependent magnetotransport properties of LVO/KTO heterostructure synthesized using pulsed laser deposition.

*Corresponding author: amitvashist42@gmail.com
†Corresponding author: suvankar.chakraverty@gmail.com

II. EXPERIMENTAL DETAILS

A PLD apparatus was used to grow crystalline LVO film (seven monolayers) on the top of a TaO_2 terminated KTO (001) single-crystal substrate [35]. During the deposition, the substrate temperature was set at 600 °C and partial oxygen pressure of 1×10^{-6} torr was maintained throughout the deposition. Then, the sample was cooled at the rate of 20 °C/min in the same oxygen partial pressure. The magnetotransport measurements were performed in the Quantum Design physical property measurement system (PPMS). Contacts were prepared at the interface with the help of an ultrasonic wire bonder in four probe (longitudinal and Hall) geometry. The current is applied parallel to the plane (001), and the angle between the current and the magnetic field was varied with the help of the horizontal rotator of PPMS.

III. RESULTS AND DISCUSSION

Figure 1(a) shows the schematic to measure the Hall resistance and magnetoresistance (MR). The longitudinal resistivity curve exhibits a metallic behavior as shown in Fig. 1(b) as it decreases with a decrease in temperature. The Hall resistance variation with the magnetic field at T= 2 K is shown in the inset of Fig. 1(b). The Hall resistance is nearly linear and the negative slope of R_{yx} suggests the electrons as a charge carrier at the interface of LVO/KTO. The variation of Hall mobility with temperature has been shown in Fig. 1(c). On fitting high magnetic field Hall resistance data with the single band model, the two-dimensional electron carrier density is found to be of the order of 10^{13} cm^{-2} and mobility of the order of 430 cm^2/V-s at 1.8 K. The mobility changes by a factor of three as the temperature changes from 1.8 K to 130 K. Careful observation shows that the Hall resistance exhibits slightly nonlinear behavior at low temperatures, indicating the presence of two conduction channels contributing to the transport properties, later confirmed by quantum oscillations and WAL data analysis. Detailed analysis of the nonlinear Hall resistance at 2 K using the two-band model [36] is shown in Sec. I of the Supplemental Material [37] (see also Refs. [38–41] therein). Figure 2(a) shows the magnetic field dependence of out-of-plane magnetoconductivity (MC) at various temperatures in the temperature range of 1.8 K to 130 K. The value of MC (or MR) decreases (increases) with an increase in temperature. The MC (or MR) shows quantum linear behavior at high field and semiclassical quadratic dependence at low field. This behavior is different from certain semimetals where MC (or MR) exhibits the convention B^2 dependence which is valid exclusively within the framework of the Drude model and demonstrates its inadequacy under conditions of elevated magnetic fields, particularly in proximity to the formation of Landau levels [42]. The transition from semiclassical to quantum can be seen more clearly from the field derivative of the MC as shown in Fig. 2(b). Initially, $d\sigma/dB$ is proportional to B, which indicates a semiclassical B^2-dependent MC. With the increase of the magnetic field, the field crosses a critical point B^* [the critical field B^* is determined from the intersection of a straight line and horizontal line as depicted in Fig. 2(b)], and $d\sigma/dB$ nearly becomes a constant as a function of the applied magnetic field. This

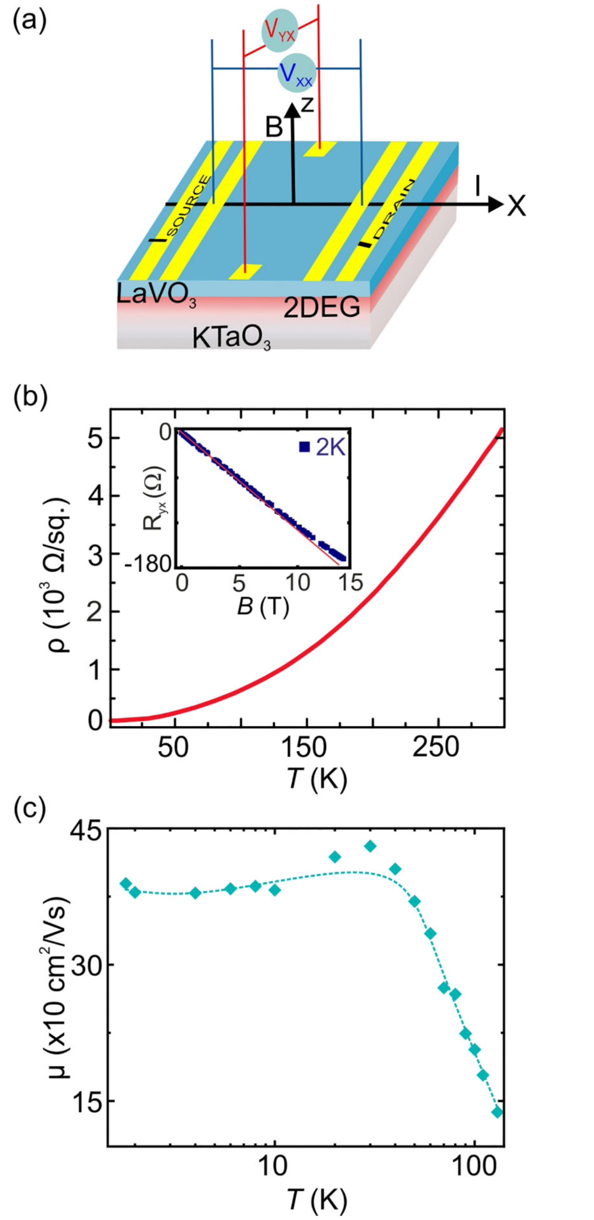

FIG. 1. (a) Schematic for Hall and in-plane magnetotransport measurements. (b) Temperature-dependent in-plane resistivity. The inset shows the variation of Hall resistance with the magnetic field at 2 K (The red line shows the deviation of Hall resistance data from a straight line). (c) Temperature-dependent mobility (blue) in $LaVO_3/KTaO_3$ heterostructure.

implies that MC (or MR) follows a linear field dependence at a high magnetic field and a quadratic field dependence at a low field. This crossover behavior gradually vanishes at T = 90 K, and the MC becomes quadratic in the entire applied magnetic field. Similarly, when we apply a magnetic field parallel to the direction of the current (i.e., $\theta = 0^\circ$), longitudinal conductivity increases with an increase in the applied magnetic field, which corresponds to negative magnetoresistance (NMR) as shown in Fig. 2(d). A similar crossover of magnetoresistance from B quadratic to B linear is observed for the applied in-plane field as well. This can be examined by observing the magnetic field derivative of conductivity,

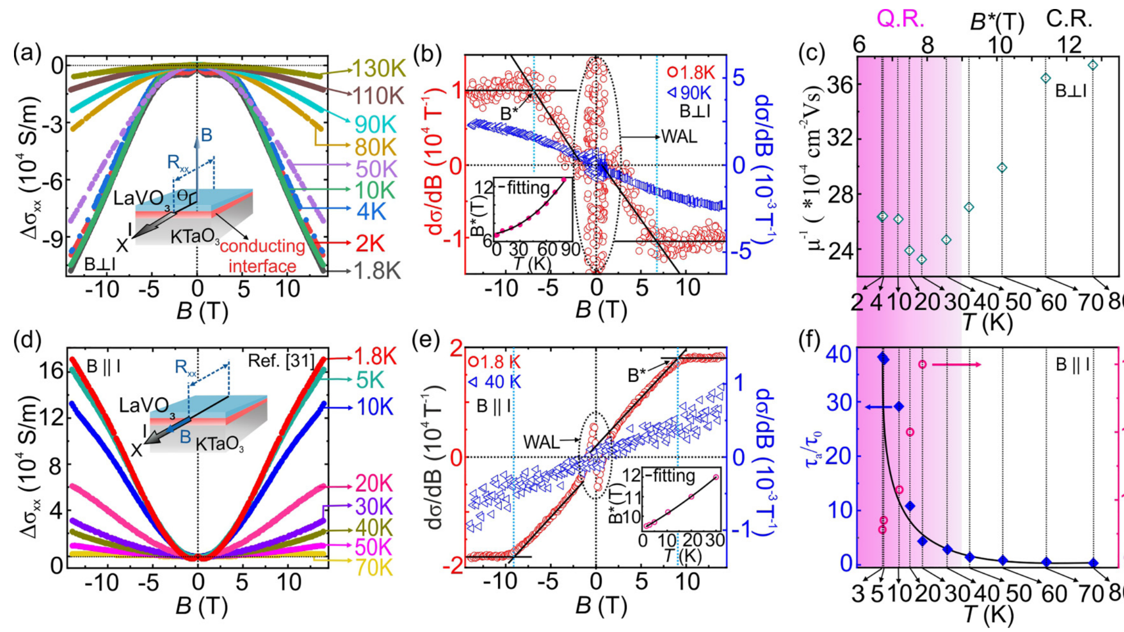

FIG. 2. (a), (d) Magnetoconductivity (MC) for B ⊥ I ($\theta = 90^{\circ}$) and B ∥ I ($\theta = 0^{\circ}$), at various temperatures. (b), (e) Variation of magnetic field derivative of conductivity with the applied magnetic field for B ⊥ I (at T = 1.8 K and 90 K) and B ∥ I (at T = 1.8 K and 40 K). Insets of both figures show the temperature dependence of critical field (B*) fitted with equation $1/(2e\hbar v_F^2)(E_F + k_BT)^2$ (black solid line). (c) Inverse Hall mobility vs crossover field B*, at various temperatures for B ⊥ I configuration. (f) Variation of the ratio of axial charge relaxation time at given field to zero field (blue rhombus), i.e., τ_a/τ_0 and crossover field B* with temperature for B ∥ I (pink open circles). The shaded region separates the quantum dominance region from the classical region.

i.e., $d\sigma/dB$ with respect to field B. The crossover behavior sustains only up to T= 30 K as shown in Fig. 2(e). Linear magnetoresistance (MR) can be attributed to two different origins: classical processes using a random resistor network and quantum effects arising when carriers condense into the lowest Landau level (LL) within the quantum limit regime. In the classical model, which describes mobility-fluctuation-induced linear magnetoresistance in an inhomogeneous conductor, the theoretical prediction indicates that the crossover field B* is inversely proportional to the mobility, i.e., ($B^* \propto \mu^{-1}$) [43]. However, in LVO/KTO, deviations from this relationship are observed, especially in the low-temperature regime as illustrated in Fig. 2(c). In a quantum model, the critical field B^* is described by the expression $B^* = 1/(2e\hbar v_F^2)(E_F + k_BT)^2$, which corresponds to the condition when all carriers degenerate into the zeroth Landau level [44]. The inset of Figs. 2(b) and 2(e) shows the parabolic dependence of the critical field on temperature, and the critical field is fitted well with the expression $1/(2e\hbar v_F^2)(E_F + k_BT)^2$ (the black solid curve). This parabolic dependence of the critical field on temperature indicates the existence of an electronic band with linear dispersion [45,46]. In addition to it, the linear MR with large carrier concentration ($\approx 10^{21}$ cm^{-3}) has been previously explained by the quantum limit model in $NbTe_2$ [47]. The high carrier concentration calculated from Hall data suggests the presence of a large Fermi surface in LVO/KTO. In addition, the LVO/KTO heterostructure also exhibits a small Fermi pocket which is supported by the quantum oscillation data. At low temperatures and large applied magnetic field, the spacing between the lowest Landau levels becomes larger than both thermal fluctuations k_BT and the Fermi energy E_F. Therefore, for a small Fermi pocket, only the lowest Landau level might be occupied, resulting in a quantum linear MR.

Another intriguing aspect of the quantum electrical transport behavior in LVO/KTO is the notable presence of SdH oscillations. These oscillations signify the crossing of Landau levels (LL) over the Fermi level as the magnetic field (B) increases. Figure 3 shows the oscillatory component of ΔR_{XX} versus 1/B at various temperatures (T) after subtracting an appropriate polynomial from the out-of-plane MR data. The amplitude of the SdH oscillations decreases with increasing T. The cross-sectional area S_F of the Fermi surface (FS) was determined utilizing the Lifshitz-Onsager relation $S_F = 2\pi eF/\hbar$. The estimated value of S_F is 3.79×10^4 Å^{-2}

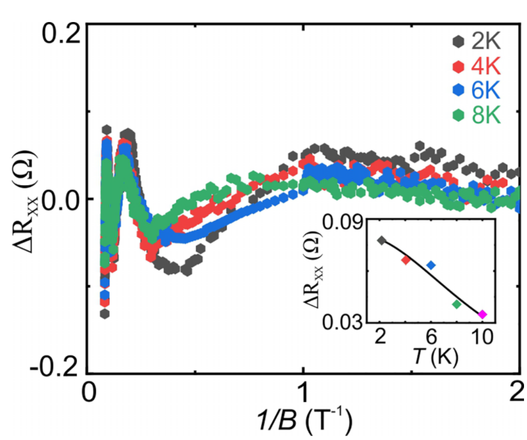

FIG. 3. The variations of ΔR_{XX} vs 1/B, after subtracting a fitted smooth background at various temperatures. Inset shows the temperature dependence of oscillation amplitudes for 10.8 T.

indicating the presence of a small Fermi pocket in the LVO/KTO heterostructure. The effective mass (i.e., $m^* = 0.18m_e$, m_e is the mass of an electron) was computed by analyzing the temperature-dependent SdH oscillation (inset of Fig. 3) amplitude at magnetic field strength 10.8 T (corresponding to first oscillation peak) and subsequently fitting the data using the formula derived from the Lifshitz-Kosevich (L-K) theory [48], $\Delta R_{XX}(T)/\Delta R_{XX}(0) = \lambda(T)/\sinh(\lambda(T))$. Here, $\lambda(T) = 2\pi^2 m^* k_B T_D/\hbar eB$, with k_B denoting Boltzmann's constant, T representing temperature, e the electric charge, and $\hbar$ (1.05×10^{-34} J-s) representing the reduced Planck's constant. In accordance with the L-K theory, the oscillation amplitude ΔR_{XX} can be expressed as $\Delta R_{XX} = 4R_0\lambda e^{-\lambda_D}/\sinh(\lambda)$. Here, R_0 represents the amplitude of the oscillation at zero magnetic field and λ_D is given by $2\pi^2 m^* k_B T_D/\hbar eB$. T_D corresponds to Dingle temperature (∼2.7 K), is given by $\hbar/2\pi k_B\tau_{SdH}$ where, τ_{SdH} is the total scattering time. Using the Dingle temperature, the value of τ_{SdH} was determined to be 0.44 ps, and using $\mu_{SdH} = e\tau/m^*$, the extracted value of quantum mobility, μ_{SdH} is ∼4349 cm^2/Vs and carrier density is $\sim 6\times10^{11}$ cm^{-2}, respectively. The prerequisites for attaining the quantum limit, which necessitate the fulfillment of two key criteria are (i) $\omega_c\tau > 1$ or ($\mu B > 1$), and (ii) $\hbar\omega_c > k_B T$. Here, ω_c signifies the cyclotron frequency, τ represents the relaxation time of carriers, μ represents the mobility of the carriers, and $k_B T$ denotes the thermal energy corresponding to temperature T. In the context of our specific investigation, we have verified the satisfaction of both these conditions. The first condition, $\omega_c\tau > 1$, is met considering the quantum mobility (μ_{SdH}) and carrier density obtained from SdH. Additionally, the second condition is also fulfilled as evidenced by $\hbar\omega_c$ with a value surpassing the thermal energy $k_B T$ at lower temperature ranges. It is worth mentioning that while the manifestation of linearity in magnetoresistance commences at approximately 7 Tesla, calculations derived from the SdH oscillations indicate that the quantum limit ought to manifest from ∼12 Tesla. This apparent incongruity presents a compelling puzzle, the resolution of which eludes our current understanding and warrants deeper investigation. Furthermore, the ratio of axial charge relaxation time at a given field to zero field, i.e., τ_a/τ_0 for various temperatures, is extracted from fitting the in-plane negative magnetoresistance (or positive MC) data with the semiclassical Boltzmann equation [49]. The variation of τ_a/τ_0 and critical field B^* for the B ∥ I configuration with temperature is illustrated in Fig. 2(f). In particular, the shaded region in Figs. 2(c) and 2(f) signifies the prevalence of quantum phenomena up to a temperature of 30 K.

It is worth mentioning that the linear magnetoresistance (MR) is evident in magnetic oxides also [50], where in-plane MR shifts from quadratic to convex with increasing magnetic field, a common pattern in magnetic oxides along the hard axis. This shift is ascribed to reduced spin scattering in the magnetic field. Conversely, the out-of-plane MR exhibits a clear linear dependence on the magnetic field, resembling the anomalous Hall effect, originating from momentum space Berry curvature. Earlier studies on disordered magnetic conductors using semiclassical Boltzmann theory with $\omega_c\tau \gg 1$ suggest that Berry curvature and associated orbital moments can induce intrinsic linear MR, observed exclusively in the out-of-plane MR when spin fluctuations are suppressed due to strong perpendicular anisotropy. However, our LVO/KTO sample interface, characterized by a nonmagnetic nature, does not manifest a comparable linear MR.

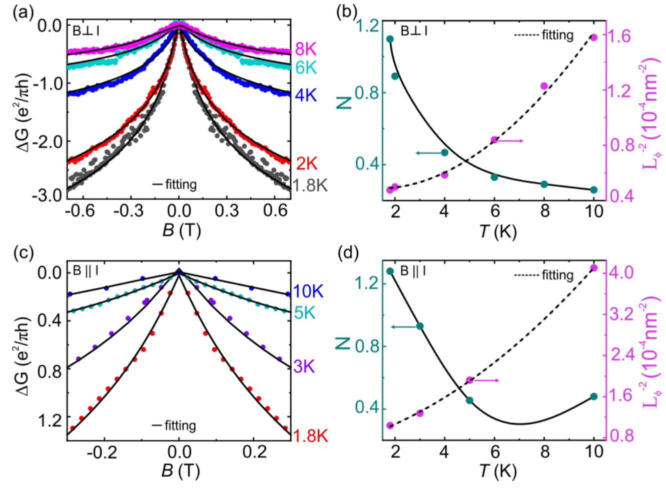

FIG. 4. (a), (c) Magnetic field dependent magneto-conductance (ΔG) data in two directions, B ⊥ I and B ∥ I, at various temperatures, fitted with the Maekawa-Fukuyama (MF) equation (fitted data is shown by black solid lines). (b), (d) Temperature dependence of N and phase coherence length L_ϕ. Fitted data is shown by a black dashed line and a solid line represents the eye-guided line.

Now we turn to the WAL analysis at the LVO/KTO interface as shown in Fig. 4. Cusplike variation under low magnetic field in Figs. 2(a) and 2(d) (around 0 T) is reminiscent of the quantum interference (QI) phenomena, i.e., WAL which is more pronounced in a magnetic field derivative of conductivity [shown by the encircled region in Figs. 2(b) and 2(e)]. WAL is observed with a magnetic field applied both in plane (0°) and out of plane (90°). As temperature increases, the cusp (indicative of WAL) is broadened and finally disappears after 8 K due to the decrease in phase coherence length L_ϕ. The dephasing length L_ϕ is the significant length scale for QI effects. L_ϕ is greater than "t" (thickness of the conducting channel) [34] in the temperature range of 10 K to 1.8 K. Typically, for such conducting interfaces the mobile charge carriers are mostly confined within around 5 nm near the interface. Therefore, we confine our analysis solely to this quasi-2D limit [51]. When we apply a magnetic field perpendicular to the plane, the Maekawa-Fukuyama (MF) formula expressed as for 2D WAL in the strong spin-orbit coupling limit gives the change in conductance as [52,53]

$$\Delta G(B) = -\left(N\frac{e^2}{\pi h}\right)\left\{F\left(\frac{B}{B_\phi + B_{so}}\right) - \frac{1}{2}\left[F\left(\frac{B}{B_\phi}\right) - F\left(\frac{B}{B_\phi + 2B_{so}}\right)\right]\right\}, \quad (1)$$

where $F(z) = \psi(\frac{1}{2} + \frac{1}{z}) + \ln(z)$, ψ is the digamma function, characteristic field $B_\phi = \hbar/(4eL_\phi^2)$, $B_{so} = \hbar/(4eL_{so})$ with L_ϕ phase coherence length, and L_{so} spin-orbit scattering length. The coefficient N gives the information regarding the number of conduction channels indulged in transport. For a single conduction channel, the value of N = 1/2, different values (N > 1/2) can be observed for more than one conduction channel, and (N < 1/2) has been observed for coexisting of topologically trivial and nontrivial conduction channels [51,54–56].

Figures 4(a) and 4(c) show the WAL effect (in the low field $|B| \leqslant 0.5$ T) for the applied magnetic field for both out-of-plane and in-plane configurations, respectively. Experimental data is fitted (as shown by the black solid line) by the MF equation [Eq. (1)] with fitting parameters N, L_ϕ, and L_{so}. The MF equation fitting yields N = 1.098 and $L_\phi = 144.8165$ nm for out-of-plane and $N = 1.2$ and $L_\phi = 98.2$ nm for in-plane configuration at 1.8 K. The temperature dependence of all derived parameters for out of plane and in plane, namely L_ϕ, L_{so}, and N, Rashba parameters (α) are given in Tables S1 and S2 in Sec. II of the Supplemental Material [37], respectively. Evidently, with increasing temperature, L_ϕ experiences a reduction due to escalated inelastic scattering effects. Conversely, L_{so} remains relatively unaltered with changing temperature, hovering at an approximate value of 6.1 nm. This is indicative of the spin-orbit field, denoted as B_{so}, which maintains a value of around 4.3 T for out of plane. The values of N are close to one, indicating the presence of two conducting channels. However, small deviations of N from one indicates that bulk bands are also contributing to transport properties. The value of coefficient N close to one has been observed in $ZrTe_5$ and $Bi_{0.95}Sb_{0.05}$ topological single crystals, etc. [56,57]. The value of N reduces with increasing temperature as shown in Figs. 4(b) and 4(d); a similar trend has been observed for several topological materials [58]. For 3D topological semimetal $Ta_{0.7}Nb_{0.3}Sb_2$, the value of N was found of the order of 102 and similar results have been observed in other 3D topological materials such that ScPdBi and YbCdGe indicate that rather than 2D surface states, 3D bulk channels dominate the magnetotransport [59–61]. However, our results indicate that the WAL at the interface of LVO/KTO is mainly due to quasi-2D conducting channels. The Nyquist theory for electron-electron (e-e) scattering gives the order of dependence of phase coherence length on temperature $L_\phi \propto T^{-1/2}$ [62]. Deviation from this suggests that e-e and electron-phonon (e-p) scattering mechanisms are present. The relation between phase coherence length with temperature is given as [63,64]

$$\frac{1}{(L_\phi)^2} = \frac{1}{(L_{\phi 0})^2} + A_{ee}T^n + B_{ep}T^{n'}, \quad (2)$$

where $L_{\phi 0}$ is the dephasing length at zero temperature, the second term is related to e-e contribution, and the third term gives the e-p interactions. The value of n′ lies in the range 2–3 as per effective dimensionality and disorder in the film [65,66]. We have obtained the best fit for $n' \sim 2$ and $n \sim 1$ [using Eq. (2)] for both in-plane and out-of-plane configurations, as shown by the dotted black line in Figs. 4(b) and 4(d), which indicates the presence of an e-p scattering mechanism. The extracted value of $A_{ee} = 2.97849 \times 10^{-6}/\text{nm}^2\text{K}$, $B_{ep} = 4.03386 \times 10^{-7}/\text{nm}^2\text{K}^2$, and $L_{\phi 0} = 157.8$ nm for out of plane and $A_{ee} = 1.39838 \times 10^{-5}/\text{nm}^2\text{K}$, $B_{ep} = 2.00354 \times 10^{-6}/\text{nm}^2\text{K}^2$, and $L_{\phi 0} = 119.1$ nm for in-plane configuration suggests the dominance of e-e scattering.

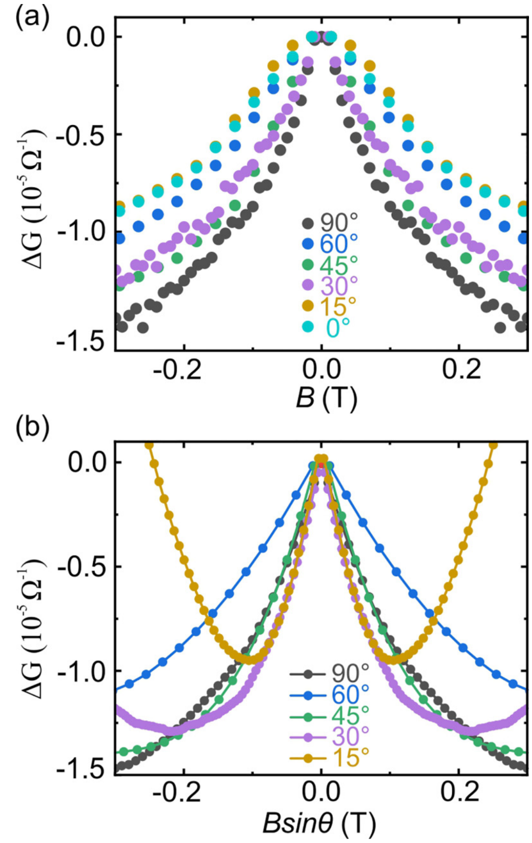

FIG. 5. (a) Magnetoconductance for different angles between the magnetic field B and the sample surface (001) at 1.8 K. (b) Magnetoconductance vs Bsinθ for different angles at 1.8 K.

To further identify the dimensionality of the charge carrier that is responsible for the WAL effect, we performed MR measurements for different angular orientations at 1.8 K. For the 2D transport only, the WAL should vanish when the angle is 0°, which is when B is along the current direction. In Fig. 5(a), the amplitude of the WAL diminishes but does not vanish completely, indicating the 3D nature of WAL [59]. In addition, if one takes the magnetoconductance as a function of the perpendicular magnetic field component Bsinθ, the amplitudes should overlap for all angles in the case of a 2D transport. Figure 5(b) shows the change in conductance (ΔG) as a function of Bsinθ, for 1.8 K, where it is possible to observe that the system does not present a pure 2D behavior as already indicated by the behavior observed in Fig. 5(a). This indicates a quasi-2D-like nature of the mobile charge carriers.

IV. CONCLUSION

In conclusion, we have observed a transition from B^2 to B linear in out of plane and in plane magnetoconductivity, might be attributed to the presence of the Dirac fermions inhabiting the lowest Landau level in the quantum limit. The critical field shows a quadratic temperature dependence which is also expected from Landau level splitting of linear energy dispersion. We have also observed the signature of WAL at the interface of LVO/KTO heterostructure. The analysis of the signature of WAL data using the MF theory suggests that multiple channels are contributing to the transport. Temperature-dependent study of dephasing length reveals that electron-electron and electron-phonon scattering contribute to phase relaxation mechanisms. At lower temperatures, the electronic transport can be treated under the framework of a charge carrier with linear band dispersion that follows a quantum framework. Angle dependence of WAL suggests a quasi-two-dimensional nature of the charge carriers. Our study shows the realization of a quasi-two-dimensional electron at the conducting interface of LVO and KTO that has nontrivial linear band dispersion and should be treated within a quantum framework at low temperature and hence opens up a new way in the field of "topological-quantum oxide materials."

ACKNOWLEDGMENTS

This project has been supported by Grant No. 01(3063)/21/EMR-II (CSIR). A.V. acknowledges the DST INSPIRE faculty fellowship (Faculty Reg. No. IFA21-PH 279) for financial support.

[1] M. Z. Hasan and C. L. Kane, *Colloquium*: topological insulators, Rev. Mod. Phys. **82**, 3045 (2010).
[2] J. E. Moore, The birth of topological insulators, Nature (London) **464**, 194 (2010).
[3] A. A. Burkov, Topological semimetals, Nat. Mater. **15**, 1145 (2016).
[4] X. Wan, A. M. Turner, A. Vishwanath, and S. Y. Savrasov, Topological semimetal and fermi-arc surface states in the electronic structure of pyrochlore iridates, Phys. Rev. B **83**, 205101 (2011).
[5] N. P. Armitage, E. J. Mele, and A. Vishwanath, Weyl and Dirac semimetals in three-dimensional solids, Rev. Mod. Phys. **90**, 015001 (2018).
[6] A. H. Castro Neto, F. Guinea, N. M. R. Peres, K. S. Novoselov, and A. K. Geim, The electronic properties of graphene, Rev. Mod. Phys. **81**, 109 (2009).
[7] K. Novoselov, A. Geim, S. V. Morozov, D. Jiang, and M. I. Grigorieva, Two-dimensional gas of massless Dirac fermions in graphene, Nature (London) **438**, 197 (2005).
[8] G. Bergmann, Weak localization in thin films: A time-of-flight experiment with conduction electrons, Phys. Rep. **107**, 1 (1984).
[9] L. P. He, X. C. Hong, J. K. Dong, J. Pan, Z. Zhang, J. Zhang, and S. Y. Li, Quantum transport evidence for the three-dimensional Dirac semimetal phase in Cd_3As_2, Phys. Rev. Lett. **113**, 246402 (2014).
[10] A. Narayanan, M. D. Watson, S. F. Blake, N. Bruyant, L. Drigo, Y. L. Chen, D. Prabhakaran, B. Yan, C. Felser, T. Kong *et al.*, Linear magnetoresistance caused by mobility fluctuations in n-doped Cd_3As_2, Phys. Rev. Lett. **114**, 117201 (2015).
[11] N. Ashcroft and N. Mermin, *Solid State Physics, HRW International Editions* (Holt, Rinehart and Winston, 1976).
[12] P. L. Rossiter and J. Bass, Electronic transport properties of normal metals, in *Materials Science and Technology* (John Wiley Sons, Ltd., 2006).
[13] H. Jin, K. Lee, S. H. Baek, J. S. Kim, B. k. Cheong, B. H. Park, S. Yoon, B. J. Suh, C. Kim, S. S. A. Seo, and S. Lee, Large linear magnetoresistance in heavily-doped Nb:$SrTiO_3$ epitaxial thin films, Sci. Rep. **6**, 34295 (2016).
[14] K. J. Kormondy, L. Gao, X. Li, S. Lu, A. B. Posadas, S. Shen, M. Tsoi, M. R. McCartney, D. J. Smith, J. Zhou, L. L. Lev, M. A. Husanu, V. N. Strocov, and A. A. Demkov, Large positive linear magnetoresistance in the two-dimensional t_{2g} electron gas at the $EuO/SrTiO_3$ interface, Sci. Rep. **8**, 7721 (2018).
[15] W. Niu, Y. Gan, Z. Wu, X. Zhang, Y. Wang, Y. Chen, L. Wang, Y. Xu, L. He, Y. Pu, and X. Wang, Large linear magnetoresistance of high-mobility 2d electron system at nonisostructural β-$Al_2O_3/SrTiO_3$ heterointerfaces, Advanced Materials Interfaces **8**, 2101235 (2021).
[16] M. M. Parish and P. B. Littlewood, Non-saturating magnetoresistance in heavily disordered semiconductors, Nature (London) **426**, 162 (2003).
[17] A. A. Abrikosov, Quantum magnetoresistance, Phys. Rev. B **58**, 2788 (1998).
[18] H. Tang, D. Liang, R. L. Qiu, and X. P. Gao, Two-dimensional transport-induced linear magneto-resistance in topological insulator Bi_2Se_3 nanoribbons, ACS Nano **5**, 7510 (2011).
[19] X. Wang, Y. Du, S. Dou, and C. Zhang, Room temperature giant and linear magnetoresistance in topological insulator Bi_2Te_3 nanosheets, Phys. Rev. Lett. **108**, 266806 (2012).
[20] Z. H. Wang, L. Yang, X. J. Li, X. T. Zhao, H. L. Wang, Z. D. Zhang, and X. P. Gao, Granularity controlled nonsaturating linear magnetoresistance in topological insulator Bi_2Te_3 films, Nano Lett. **14**, 6510 (2014).
[21] Y. Yan, L. X. Wang, D. P. Yu, and Z. Liao, Large magnetoresistance in high mobility topological insulator Bi_2Se_3, Appl. Phys. Lett. **103**, 033106 (2013).
[22] J. Fujioka, R. Yamada, M. Kawamura, S. Sakai, M. Hirayama, R. Arita, T. Okawa, D. Hashizume, M. Hoshino, and Y. Tokura, Strong-correlation induced high-mobility electrons in Dirac semimetal of perovskite oxide, Nat. Commun. **10**, 362 (2019).
[23] J. Shiogai, T. Chida, K. Hashimoto, K. Fujiwara, T. Sasaki, and A. Tsukazaki, Signature of band inversion in the perovskite thin-film alloys $BaSn_1 - xPb_xO_3$, Phys. Rev. B **101**, 125125 (2020).
[24] Z. Liu, M. Li, Q. Li, J. Liu, W. Li, H. Yang, Q. Yao, C. Fan, X. Wan, Z. Wang *et al.*, Direct observation of the Dirac nodes lifting in semimetallic perovskite $SrIrO_3$ thin films, Sci. Rep. **6**, 30309 (2016).
[25] K. Takiguchi, Y. K. Wakabayashi, H. Irie, Y. Krockenberger, T. Otsuka, H. Sawada, S. A. Nikolaev, H. Das, M. Tanaka, Y. Taniyasu *et al.*, Quantum transport evidence of Weyl fermions in an epitaxial ferromagnetic oxide, Nat. Commun. **11**, 4969 (2020).
[26] T. C. Asmara, D. Wan, Y. Zhao, M. A. Majidi, C. T. Nelson, M. C. Scott, Y. Cai, B. Yan, D. Schmidt, M. Yang *et al.*, Tunable and low-loss correlated plasmons in Mott-like insulating oxides, Nat. Commun. **8**, 15271 (2017).
[27] N. Wadehra, R. Tomar, R. M. Varma, R. K. Gopal, Y. Singh, S. Dattagupta, and S. Chakraverty, Planar hall effect and anisotropic magnetoresistance in polar-polar interface of $LaVO_3$-$KTaO_3$ with strong spin-orbit coupling, Nat. Commun. **11**, 874 (2020).

[28] S. Goyal, N. Wadehra, and S. Chakraverty, Tuning the electrical state of 2DEG at $LaVO_3$-$KTaO_3$ interface: effect of light and electrostatic gate, Adv. Mater. Interfaces **7**, 2000646 (2020).

[29] M. Dumen, A. Singh, S. Goyal, C. Bera, and S. Chakraverty, Photoconductivity of the EuO-KTO interface: Effect of intrinsic carrier density and temperature, J. Phys. Chem. C **125**, 15510 (2021).

[30] H. Y. Hwang, Y. Iwasa, M. Kawasaki, B. Keimer, N. Nagaosa, and Y. Tokura, Emergent phenomena at oxide interfaces, Nat. Mater. **11**, 103 (2012).

[31] A. Ohtomo and H. Y. Hwang, A high-mobility electron gas at the $LaAlO_3/SrTiO_3$ heterointerface, Nature (London) **427**, 423 (2004).

[32] N. Kumar, N. Wadehra, R. Tomar, Shama, S. Kumar, Y. Singh, S. Dattagupta, and S. Chakraverty, Observation of shubnikov–de haas oscillations, planar hall effect, and anisotropic magnetoresistance at the conducting interface of $EuO-KTaO_3$, Adv. Quantum Technol. **4**, 2000081 (2021).

[33] S. Chakraverty, T. Matsuda, H. Wadati, J. Okamoto, Y. Yamasaki, H. Nakao, Y. Murakami, S. Ishiwata, M. Kawasaki, Y. Taguchi, Y. Tokura, and H. Y. Hwang, Multiple helimagnetic phases and topological hall effect in epitaxial thin films of pristine and co-doped $SrFeO_3$, Phys. Rev. B **88**, 220405(R) (2013).

[34] H. Silotia, A. Kumari, A. Gupta, J. De, S. K. Pal, R. Tomar, and S. Chakraverty, Possible signatures of chiral anomaly in the magnetoresistance of a quasi-2-dimensional electron gas at the interface of $LaVO_3$ and $KTaO_3$, Adv. Electron. Mater. **8**, 2200195 (2022).

[35] R. Tomar, N. Wadehra, V. Budhiraja, B. Prakash, and S. Chakraverty, Realization of single terminated surface of perovskite oxide single crystals and their band profile: $(LaAlO_3)_{0.3}(Sr_2AlTaO_6)_{0.7}$, $SrTiO_3$ and $KTaO_3$ case study, Appl. Surf. Sci. **427**, 861 (2018).

[36] H. Rotella, O. Copie, A. Pautrat, P. Boullay, A. David, D. Pelloquin, C. Labbé, C. Frilay, and W. Prellier, Two components for one resistivity in $LaVO_3$-$SrTiO_3$ heterostructure, J. Phys.: Condens. Matter **27**, 095603 (2015).

[37] See Supplemental Material at http://link.aps.org/supplemental/10.1103/PhysRevB.109.245405 for the analysis of nonlinear Hall resistance using the two-band model, with Maekawa-Fukuyama (MF) equation fitting parameters.

[38] Y. Hotta, T. Susaki, and H. Y. Hwang, Polar discontinuity doping of the $LaVO_3$-$SrTiO_3$ interface, Phys. Rev. Lett. **99**, 236805 (2007).

[39] C. Bell, S. Harashima, Y. Kozuka, M. Kim, B. G. Kim, Y. Hikita, and H. Y. Hwang, Dominant mobility modulation by the electric field effect at the $LaAlO_3$-$SrTiO_3$ interface, Phys. Rev. Lett. **103**, 226802 (2009).

[40] J. S. Kim, S. S. A. Seo, M. F. Chisholm, R. K. Kremer, H.-U. Habermeier, B. Keimer, and H. N. Lee, Nonlinear hall effect and multichannel conduction in $LaTiO_3$-$SrTiO_3$ superlattices, Phys. Rev. B **82**, 201407(R) (2010).

[41] A. Kumari, J. De, S. Dattagupta, H. N. Ghosh, S. K. Pal, and S. Chakraverty, Probing conducting interfaces by combined photoluminescence and transport measurements: $LaVO_3$-$SrTiO_3$ interface as a case study, Phys. Rev. B **104**, L081111 (2021).

[42] K. K. Huynh, Y. Tanabe, and K. Tanigaki, Both electron and hole Dirac cone states in $Ba(FeAs)_2$ confirmed by magnetoresistance, Phys. Rev. Lett. **106**, 217004 (2011).

[43] X. Z. Xing, C. Q. Xu, N. Zhou, B. Li, J. Zhang, Z. X. Shi, and X. Xu, Large linear magnetoresistance in a transition-metal stannide β-$RhSn_4$, Appl. Phys. Lett. **109**, 122403 (2016).

[44] S. Zhang, L. Yan, J. Qi, M. Zhuo, Y. Q. Wang, R. Prasankumar, Q. Jia, and S. Picraux, Epitaxial thin films of topological insulator Bi_2Te_3 with two-dimensional weak anti-localization effect grown by pulsed laser deposition, Thin Solid Films **520**, 6459 (2012).

[45] Shama, D. Dixit, G. Sheet, and Y. Singh, Unusual magnetotransport from two-dimensional Dirac fermions in $Pd_3Bi_2Se_2$, Physica E **144**, 115457 (2022).

[46] Y.-Y. Wang, Q. H. Yu, and T. L. Xia, Large linear magnetoresistance in a new Dirac material $BaMnBi_2$, Chin. Phys. B **25**, 107503 (2016).

[47] H. Chen, Z. Li, X. Fan, L. Guo, and X. Chen, Quantum linear magnetoresistance in $NbTe_2$, Solid State Commun. **275**, 16 (2018).

[48] O. Pavlosiuk, D. Kaczorowski, and P. Wiśniewski, Shubnikov - de haas oscillations, weak antilocalization effect and large linear magnetoresistance in the putative topological superconductor lupdbi, Sci. Rep. **5**, 9158 (2015).

[49] J. Xiong, S. K. Kushwaha, T. Liang, J. W. Krizan, M. Hirschberger, W. Wang, R. J. Cava, and N. P. Ong, Evidence for the chiral anomaly in the Dirac semimetal Na_3Bi, Science **350**, 413 (2015).

[50] X. Chen, X. Zhang, M. G. Han, L. Zhang, Y. Zhu, X. Xu, and X. Hong, Magnetotransport anomaly in room-temperature ferrimagnetic $NiCo_2O_4$ thin films, Adv. Mater. **31**, 1805260 (2019).

[51] B. Zhao, P. Cheng, H. Pan, S. Zhang, B. Wang, G. Wang, F. Xiu, and F. Song, Weak antilocalization in Cd_3As_2 thin films, Sci. Rep. **6**, 22377 (2016).

[52] S. Maekawa and H. Fukuyama, Magnetoresistance in two-dimensional disordered systems: Effects of zeeman splitting and spin-orbit scattering, J. Phys. Soc. Jpn. **50**, 2516 (1981).

[53] Z. Li, D. Guo, K. Huang, G. Ma, X. Liu, Y. Wu, J. Yuan, Z. Tao, B. Wang, X. Wang, Z. Zou, N. Yu, G. Yu, J. Xue, Z. Liu, W. Ji, J. Li, and Y. Guo, Robust weak antilocalization effect up to $\beta 120\,k$ in the van der waals crystal $Fe_5 - xGeTe_2$ with near-room-temperature ferromagnetism, J. Phys. Chem. Lett. **14**, 5456 (2023).

[54] Z. Li, I. Garate, J. Pan, X. Wan, T. Chen, W. Ning, X. Zhang, F. Song, Y. Meng, X. Hong, X. Wang, L. Pi, X. Wang, B. Wang, S. Li, M. A. Reed, L. Glazman, and G. Wang, Experimental evidence and control of the bulk-mediated intersurface coupling in topological insulator Bi_2Te_2Se nanoribbons, Phys. Rev. B **91**, 041401(R) (2015).

[55] H. Z. Lu and S. Q. Shen, Weak localization of bulk channels in topological insulator thin films, Phys. Rev. B **84**, 125138 (2011).

[56] Y. Kumar and V. P. S. Awana, Weak anti-localization effect and study of de-phasing mechanism in $Bi_{0.95}Sb_{0.05}$ topological single crystal, J. Supercond. Novel Magn. **34**, 1303 (2021).

[57] Z. Xie, X. Wei, S. Cao, Y. Zhang, S. Yan, G. D. Gu, Q. Li, and J. H. Chen, Electron-electron interactions and weak antilocalization in few-layer $ZrTe_5$ devices, Phys. Rev. B **103**, 155408 (2021).

[58] Shama, R. K. Gopal, G. Sheet, and Y. Singh, 2D weak antilocalization in thin films of the topological semimetal $Pd_3Bi_2S_2$, Sci. Rep. **11**, 12618 (2021).

[59] M. Xu, L. Guo, L. Chen, Y. Zhang, S. S. Li, W. Zhao, X. Wang, S. Dong, and R. K. Zheng, Emerging weak antilocalization effect in $Ta_{0.7}Nb_{0.3}Sb_2$ semimetal single crystals, Front. Phys. **18**, 13304 (2023).

[60] J. Zhang, Z. Hou, C. Zhang, J. Chen, P. Li, Y. Wen, Q. Zhang, W. Wang, and X. Zhang, Weak antilocalization effect and high-pressure transport properties of ScPdBi single crystal, Appl. Phys. Lett. **115**, 172407 (2019).

[61] A. Laha, S. Malick, R. Singha, P. Mandal, P. Rambabu, V. Kanchana, and Z. Hossain, Magnetotransport properties of the correlated topological nodal-line semimetal YbCdGe, Phys. Rev. B **99**, 241102(R) (2019).

[62] C. Y. Wu, B. T. Lin, Y. J. Zhang, Z. Q. Li, and J. J. Lin, Electron dephasing in homogeneous and inhomogeneous indium tin oxide thin films, Phys. Rev. B **85**, 104204 (2012).

[63] J. J. Lin and J. Bird, Recent experimental studies of electron dephasing in metal and semiconductor mesoscopic structures, J. Phys.: Condens. Matter **14**, R501 (2002).

[64] S. Islam, S. Bhattacharyya, H. Nhalil, M. Banerjee, A. Richardella, A. Kandala, D. Sen, N. Samarth, S. Elizabeth, and A. Ghosh, Low-temperature saturation of phase coherence length in topological insulators, Phys. Rev. B **99**, 245407 (2019).

[65] M. Y. Reizer and A. V. Sergeyev, Electron-phonon interaction in impure metals and superconductors, Sov. J. Exp. Theor. Phys. **63**, 616 (1986).

[66] N. P. Breznay, H. Volker, A. Palevski, R. Mazzarello, A. Kapitulnik, and M. Wuttig, Weak antilocalization and disorder-enhanced electron interactions in annealed films of the phase-change compound $GeSb_2Te_4$, Phys. Rev. B **86**, 205302 (2012).